RPC Estimation via ℓ_1-Norm-Regularized Least Squares (L1LS)

Tengfei Long, Weili Jiao, and Guojin He

***Abstract*—A rational function model (RFM), which consists of 80 rational polynomial coefficients (RPCs), has been widely used to take the place of rigorous sensor models in photogrammetry and remote sensing. However, it is difficult to solve the RPCs because of the requirement for numerous observation data [ground control points (GCPs)] in a terrain-dependent case and the strong correlation between the coefficients (ill-poseness). Regularization methods are usually applied to cope with the correlations between the coefficients, but only ℓ_2-norm regularization is used by the existing approaches (e.g., ridge estimation and Levenberg–Marquardt method). The ℓ_2-norm regularization can make an ill-posed problem well-posed but does not reduce the requirement for observation data. This paper presents a novel approach to estimate RPCs using ℓ_1-norm-regularized least squares (L1LS), which provides stable results not only in a terrain-dependent case but also in a terrain-independent case. On one hand, by means of L1LS, the terrain-dependent RFM becomes practical as reliable RPCs can be obtained by using much less than 40 or 39 (if the first denominators are equal to 1) GCPs, without knowing the orientation parameters of the sensor. On the other hand, the proposed method can be applied to directly refine the terrain-independent RPCs with additional GCPs: when a single or several GCPs are used, direct refinement performs similarly to bias compensation in image space; when more GCPs are available, the direct refinement can achieve comparable accuracy of the rigorous sensor model (better than conventional bias compensation in image space).**

***Index Terms*—Compressive sensing, Lasso via the least angle regression (LARS), least absolute shrinkage and selection operator (Lasso), rational polynomial coefficients (RPCs), variable selection, ℓ_1-norm regularization.**

I. Introduction

EARTH observation optical sensors mounted on satellites use mainly charge-coupled device (CCD) linear arrays and pushbroom mode acquisition [1]. The rigorous sensor model of the pushbroom sensors is complicated as each line of a pushbroom satellite image has different exposure stations and orientations [2], and the model can be variable when considering the possible lens distortions and CCD line distortions. Moreover, rigorous sensor models differ from each other among different satellite sensors, and it is expensive, time-consuming, and error prone for users to build a complicated rigorous sensor model for each satellite sensor. Fortunately, the rational function model (RFM) [3] provides a standard and easy approach for photogrammetric mapping from remotely sensed images. RFM, whose parameters are called rational polynomial coefficients (RPCs), is a generalized imaging geometry model which is recommended by the Open GIS Consortium [4] and has been widely used to process high-resolution satellite images. By utilizing RFM, it is possible to perform orthocorrection (given a DEM) or some 3-D operations like building height computation from the remotely sensed images without knowing the ephemeris, attitude, or other parameters of the satellites and sensors. As a matter of fact, most of the modern high-resolution satellite products are distributed with RPCs, including products from ALOS, GeoEye, DigitalGlobe, Pleiades, SPOT-6/7, ZY-3, GF-1/2, etc. Users can directly perform geometric processing on these products with the provided RPCs and also further refine the RFM using several additional ground control points (GCPs) [5]–[8], or digital elevation models [9].

However, RFM also has several disadvantages: 1) As the full RFM contains 80 RPCs, at least 40 or 39 (if the first denominators are equal to 1) GCPs are required to solve the RPCs; 2) the 80 RPCs of RFM are usually strongly correlated, and the estimation of RPCs is an ill-posed problem; 3) the RFM is a mathematical model independent from the physical imaging process and is interpretable; and 4) the RFM is applicable to a photogrammetric camera with a narrow field of view, calibrated, and stable interior orientation [10] but does not necessary have a good performance for the camera with a wide field of view or the unstable interior orientation.

Generally, the RPCs of the RFM can be solved with or without knowing the rigorous sensor models. If the rigorous sensor model is available, the terrain-independent solution can be developed. Otherwise, the RFM solution will be highly terrain-dependent [11]. The application of RFM in the modern high-resolution satellite image products with provided RPCs is successful as the RPCs are solved terrain independently with the rigorous sensor models. In the terrain-independent case, GCPs are virtually generated from the rigorous sensor model, and abundant GCPs are always available; when four or more elevation layers in the object grid are used, the normal equation is less likely to be ill-conditioned. Moreover, as the high-resolution satellite images are usually captured by narrow

Manuscript received February 28, 2014; revised November 30, 2014 and January 4, 2015; accepted January 23, 2015. This work was supported by a grant from the National Natural Science Foundation of China (61271013), the National High Technology Research and Development Program of China (2012BAH27B05), and 135 Strategy Planning of Institute of Remote Sensing and Digital Earth, Chinese Acacemy of Sciences (CAS) and Director Foundation of Institute of Remote Sensing and Digital Earth, CAS for Graduate (Y3ZZ18101B). (*Corresponding author: Guojin He*).

T. Long is with the Institute of Remote Sensing and Digital Earth (RADI), Chinese Academy of Sciences, Beijing 100094 China, and also with the University of Chinese Academy of Sciences, Beijing 100049 China.

W. Jiao and G. He are with the Institute of Remote Sensing and Digital Earth (RADI), Chinese Academy of Sciences, Beijing 100094 China (e-mail: gjhe@ceode.ac.cn).

Color versions of one or more of the figures in this paper are available online at http://ieeexplore.ieee.org.

Digital Object Identifier 10.1109/TGRS.2015.2401602

field-of-view cameras, RFM can precisely approximate the rigorous sensor models. The terrain-dependent RFM, on the other hand, is hardly used because of the requirement for numerous GCPs and the strong correlation between the coefficients. Additionally, RFM is also seldom applied in wide field-of-view cameras.

The key difficulty for utilizing RFM is to solve the RPCs robustly from the ill-posed normal equation. "Variational regularization [12]" and "variable selection [13]" are two standard techniques for improving ordinary least squares (OLS) and dealing with ill-posed problems. Regularization methods are usually applied to make an ill-posed problem well-posed [12], and many regularization approaches, including Tikhonov regularization, ridge estimation, and Levenberg–Marquardt method, have been used to estimate the RPCs of RFM. These regularization techniques can prevent overfitting and therefore make the model less ill-posed; however, they still require numerous GCPs, and the solution may be oscillatory if the observations are insufficient. On the other hand, some researchers have also tried to achieve a stable and reliable solution of RPCs and obtain parsimonious models via variable selection [14]–[16]. The full process of selecting the best variable subset requires exhaustive searches over all subsets, and it is combinatorial in nature and has exponential complexity. Greedy search strategy is usually used to reduce the searching cost, but it can be extremely variable because it is a discrete process. More reviews about the techniques copping with ill-posed problems can be found in [16]. It can be seen that the ordinary techniques of variational regularization and variable selection are not robust enough for practical RPC estimation.

Considering that the ill-poseness of the model results from the multicollinearity between the RPCs, some of the RPCs should be omitted to make the model more stable. Motivated by the concept of compressive sensing or compressive sampling [17]–[19], we consider the RPCs as a sparse vector with several zero elements, and the RFM may be reconstructed almost losslessly from much less observations than those required in OLS. By virtual use of the theory of compressive sensing, the variable selection problem (i.e., ℓ_0-norm minimization problem) can be solved by ℓ_1-norm-regularized least squares (L1LS) equivalently [17], [18]. Moreover, some available techniques of ℓ_1-norm regularization (such as least absolute shrinkage and selection operator (Lasso) [20], basis pursuit denoising [21], least angle regression (LARS) [22], elastic net [23], etc.) make it possible to find the unique solution of RPCs from insufficient observations efficiently and robustly.

The remainder of this paper is organized as follows. In Section II, variational regularizations based on ℓ_0-norm, ℓ_1-norm, and ℓ_2-norm are introduced, and then, a robust RPC estimating method is proposed in Section III. In Section IV, several experiments are carried out using the proposed approach. Finally, Section V concludes with some discussions.

II. Variational Regularization

First, we consider a standard linear Gauss–Markov model as

$$\mathbf{L} = \mathbf{A}\mathbf{x} + \mathbf{V} \tag{1}$$

where $\mathbf{L} \in \mathbf{R}^m$ is the vector of observations, $\mathbf{A} \in \mathbf{R}^{m\times n}$ is the data matrix, $\mathbf{x} \in \mathbf{R}^n$ is the vector of unknowns, and $\mathbf{V} \in \mathbf{R}^m$ is the vector of random errors.

When $m \geq n$ and the columns of $\mathbf{A}$ are linearly independent, $\mathbf{x}$ can be uniquely determined by OLS estimation. However, when the columns of $\mathbf{A}$ are multicollinear or the number of observations m is not large enough compared to n, OLS leads to overfitting, and the solution may be quite oscillatory or even not unique.

A. ℓ_2-Norm

A standard technique to prevent overfitting is ℓ_2-norm or Tikhonov regularization [24], which can be written as

$$\min_{\mathbf{x}\in\mathbf{R}^n} \|\mathbf{A}\mathbf{x} - \mathbf{L}\|_2^2 + \lambda\|\mathbf{x}\|_2^2 \tag{2}$$

where $\|\mathbf{x}\|_2 := (\sum_i x_i^2)^{1/2}$ is the ℓ_2-norm of $\mathbf{x}$ and $\lambda > 0$ is the regularization parameter. This ℓ_2-norm-regularized least squares problem can be solved analytically as

$$\hat{\mathbf{x}}_{\ell_2} = (\mathbf{A}^\top\mathbf{A} + \lambda\mathbf{I})^{-1}\mathbf{A}^\top\mathbf{L} \tag{3}$$

where $\mathbf{I}$ is an $n \times n$ identity matrix.

Equation (3) is also well known as "ridge estimation," which has been widely used to estimate the RPCs. Determination of the regularization parameter λ is nontrivial. Typically, solutions are computed for a large number of different λ values, and the best one is selected by suitable heuristics, e.g., the L-curve-based method [11].

Obviously, the solution $\hat{\mathbf{x}}_{\ell_2}$ of ℓ_2-norm-regularized least squares estimation is a linear function of $\mathbf{L}$ and is easy to compute. However, only when $\lambda \to \infty$, the optimal solution $\hat{\mathbf{x}}_{\ell_2}$ tends to zero. In other words, ℓ_2-norm-regularized least squares estimation does not perform variable selection.

B. ℓ_0-Norm

When the number of observations $m < n$, the columns of $\mathbf{A}$ are linearly dependent, and the OLS solution is not unique. To get a unique solution, one has to choose an optimized subset from the variable set, which is also the minimizer of ℓ_0-norm-regularized least squares as [17], [25]

$$\min_{\mathbf{x}\in\mathbf{R}^n} \|\mathbf{A}\mathbf{x} - \mathbf{L}\|_2^2 + \lambda\|\mathbf{x}\|_0 \tag{4}$$

where $\|\mathbf{x}\|_0 := \mathbf{card}(\{i : x_i \neq 0\})$ is the ℓ_0-norm of $\mathbf{x}$ and $\lambda > 0$ is the regularization parameter. $\mathbf{card}(\cdot)$ stands for cardinality of a set.

ℓ_0-norm regularization directly makes some of the variables zero, therefore obtaining a unique solution even when $m < n$. However, solving this problem essentially requires exhaustive searches over all subsets of columns of $\mathbf{A}$, a procedure which is combinatorial in nature and has exponential complexity.

C. ℓ_1-Norm

Another technique to regularize an ill-posed problem is to use ℓ_1-norm constraints as

$$\min_{\mathbf{x}\in\mathbf{R}^n} \|\mathbf{A}\mathbf{x} - \mathbf{L}\|_2^2 + \lambda\|\mathbf{x}\|_1 \tag{5}$$

where $\|\mathbf{x}\|_1 := \sum_i |x_i|$ is the ℓ_1-norm of $\mathbf{x}$ and $\lambda > 0$ is the regularization parameter.

Note that ℓ_1-norm-regularized least squares estimation typically yields a sparse vector $\mathbf{x}$ which has only a few nonzero elements. In contrast, the solution $\hat{\mathbf{x}}_{\ell_2}$ to the ℓ_2-norm regularization problem typically has all elements nonzero [24]. As a matter of fact, [26] has shown exact equivalence between the ℓ_0-norm minimization and ℓ_1-norm minimization. Moreover, although the solution of ℓ_1-norm-regularized least squares estimation is not a linear function of $\mathbf{L}$, unlike the ℓ_0-norm which enumerates the nonzero elements, the ℓ_1-norm is convex. Moreover, the ℓ_1-norm-regularized least squares problem can be transformed to a convex quadratic problem, with linear inequality constraints [27] as

$$\min_{\mathbf{x}\in\mathbf{R}^n} \|\mathbf{A}\mathbf{x} - \mathbf{L}\|_2^2 \quad \text{subject to } \|\mathbf{x}\|_1 \le \alpha. \tag{6}$$

Note that α is inversely related to λ in (5) [28]. This equivalent quadratic program can be solved by standard convex optimization methods.

III. Robust RPC Estimation

A. RFM and the Linearized Form

The RFM is a mathematical model, in which image pixel coordinates are expressed as the ratios of the polynomials of the ground coordinates. For the ground-to-image transformation, the defined ratios of the polynomials have the form as [4]

$$l = \frac{N_l(X,Y,Z)}{D_l(X,Y,Z)} \qquad s = \frac{N_s(X,Y,Z)}{D_s(X,Y,Z)} \tag{7}$$

where

- (l, s) normalized line and sample coordinates in image space;
- (X, Y, Z) normalized coordinates of ground points in object space;

$$\begin{aligned} N_l(X,Y,Z) = {} & a_0 + a_1X + a_2Y + a_3Z + a_4XY \\ & + a_5XZ + a_6YZ + a_7X^2 + a_8Y^2 \\ & + a_9Z^2 + a_{10}XYZ + a_{11}X^3 + a_{12}XY^2 \\ & + a_{13}XZ^2 + a_{14}X^2Y + a_{15}Y^3 \\ & + a_{16}YZ^2 + a_{17}X^2Z + a_{18}Y^2Z + a_{19}Z^3; \end{aligned}$$

$$D_l(X,Y,Z) = b_0 + b_1X + b_2Y + b_3Z + \cdots + b_{19}Z^3;$$

$$N_s(X,Y,Z) = c_0 + c_1X + c_2Y + c_3Z + \cdots + c_{19}Z^3;$$

$$D_s(X,Y,Z) = d_0 + d_1X + d_2Y + d_3Z + \cdots + d_{19}Z^3;$$

- a_i, b_i, c_i, d_i $(i = 0, 1, \ldots, 19)$ RPCs, and b_0 and d_0 are commonly set to 1. When b_0 and d_0 are not equal to 1, one can divide each line coefficient by b_0 and each sample coefficient by d_0 to obtain a group of equivalent RPCs, in which the new b_0 and d_0 are 1.

Although it is a nonlinear model, the RFM can be transformed into a linear model by a simple deformation, and the deformed linear model is shown as

$$\begin{aligned} N_l(X,Y,Z) - lD_l(X,Y,Z) &= 0 \\ N_s(X,Y,Z) - sD_s(X,Y,Z) &= 0. \end{aligned} \tag{8}$$

Then, the observation equations of n GCPs can be written in the same form as (1), whose elements are specified as follows:

$$\begin{aligned} \mathbf{L} &= [l_1, l_2, \ldots, l_n, s_1, s_2, \ldots, s_n]^\top; \\ \mathbf{x} &= [a_0, \ldots, a_{19}, b_1, \ldots, b_{19}, c_0, \ldots, c_{19}, d_1, \ldots, d_{19}]^\top; \\ \mathbf{A} &= [\mathbf{A}_1, \mathbf{A}_2, \ldots, \mathbf{A}_n]^\top; \\ \mathbf{A}_i &= [1, X_i, Y_i, \ldots, Z_i^3, -l_iX_i, -l_iY_i, \ldots, -l_iZ_i^3, \\ &\qquad 1, X_i, Y_i, \ldots, Z_i^3, -s_iX_i, -s_iY_i, \ldots, -s_iZ_i^3]^\top; \end{aligned}$$

- (l_i, s_i) normalized line and sample coordinates of the ith GCP in image space;
- (X_i, Y_i, Z_i) normalized coordinates of the ith GCP in object space;
- $i = 1, 2, \ldots, n$.

B. RPC Estimation via ℓ_1-Norm Regularization

As introduced in Section I, the multicollinearity between the RPCs makes the model ill-posed, and some of the RPCs should be omitted to make the model more stable. Reference [16] has proposed a method named NRBOS to select the important RPCs automatically and achieved reasonable results. NRBOS actually performs forward selection [29] with some goodness-of-fit criterion over the RPCs, and it may be overly greedy, and therefore, the result is unstable and is not optimal sometimes. Ridge estimation (the solution of ℓ_2-norm-regularized least squares estimation), which has been widely utilized to estimate RPCs, does not perform variable selection and commonly fails to yield a reasonable result when the number of GCPs is not enough compared to the number of RPCs. ℓ_1-norm-regularized least squares estimation, however, has some of the favorable properties of both variable selection and ridge estimation: it produces parsimonious models like variable selection and exhibits the stability of ridge estimation [20].

The ℓ_1-norm-regularized problem is convex, guaranteeing the global optimizer, but not differentiable. The nondifferentiable constraints can be converted into a set of linear constraints, and thus, the feasible region forms a polyhedron. Many approaches have been introduced to solve the problem, such as Lasso [20], interior point method [21], [24], active set method [30], iterated ridge regression [31], grafting [32], etc. In this paper, the Lasso via the LARS algorithm [22], [33], [34] is employed. LARS is similar to forward selection [29], which includes one variable at each step, but the value of the estimated

variables is increased in a direction equiangular to each one's correlations with the residual. Therefore, it has the same order of computation as an OLS fit applied to the full set of covariates. Test results show that the OLS spent 0.027 s to calculate the RPCs on the personal computer using $5 \times 15 \times 15$ 3-D control grid points (2250 equations), while the proposed method spent 0.078 s to do the same thing. Obviously, the computation cost of the method would not be the bottleneck of practical applications.

Retrospecting the ℓ_1-norm-regularized least squares estimation in (5), an optimal regularization parameter λ is usually searched via generalized cross-validation (GCV), which does not always yield good regularization parameters when available observations are relatively insufficient. Contrastingly, for the particular problem of solving RPCs, empirical parameters practically provide more robust results. A value in the range of $10^{-5} \sim 10^{-4}$ commonly performs well in numerous experiments carried out by the authors.

The workflow of estimating RPCs using ℓ_1-norm-regularized least squares (L1LS) can be summarized as Procedure 1.

Procedure 1 RPC Estimation via ℓ_1-Norm Regularization

Input: n GCPs and the parameter λ
RPCs estimation:
1: Normalize the coordinates;
2: Reform the RFM by Equation (7) to get a linear model as Equation (1);
3: Get a ℓ_1-norm-regularized least squares as formula (5);
4: Estimate RPCs using Lasso via LARS algorithm [34].
Output: Sparse RPCs with several possible zero coefficients.

Note that Procedure 1 does not require as many GCPs (commonly much more than 39 GCPs) to solve the 78 RPCs stably as the conventional approaches (e.g., OLS, ridge estimation, etc.) do, and sparse RPCs can even be obtained by using less than 39 GCPs.

C. Applications

1) Terrain-Dependent Case: The application of terrain-dependent RFM is generally limited because of the requirement for numerous GCPs and the unsuitability resulting from the strong correlation between the coefficients. However, the proposed approach to solve RPCs via L1LS can provide robust RPCs even when GCPs are insufficient comparing to the 78 unknown coefficients. Consequently, the terrain-dependent RFM can become practical owing to the ℓ_1-norm regularization, and some verification tests will be carried out in Section IV.

2) Terrain-Independent Case: Although the terrain-independent RFM has been widely and successfully applied in modern high-resolution satellite image products, the proposed approach can also benefit the application of terrain-independent RFM. First, L1LS provides a more robust approach to produce terrain-independent RPCs from the rigorous sensor model. Second, it becomes possible to refine the provided RPCs with several additional GCPs. Note that the existing RPC refining methods just do bias compensation in image space [6], [35] or in the orbital space [36], while our approach directly makes correction on all possible coefficients.

The terrain-independent RPCs are estimated using the 3-D grid points generated from the rigorous sensor model, without GCPs. The terrain-independent RFM can approximate the rigorous sensor model quite well but also inherits the systematic errors of the rigorous sensor model, e.g., biases of position and attitude data which are directly observed using onboard GPS receivers, gyros, and star trackers. Ideally, these positional biases are for all practical purposes invariant throughout the scene, and they can be modeled in either object space or image space, with the most practical approach being via shifts in the line and sample coordinates [3]. However, other potential biases, such as the possible lens distortions and CCD line distortions, the effect of atmospheric conditions, etc., may not be modeled by simple transformations in image space or ground space. Consequently, direct refinement of RPCs can be useful to achieve better accuracy than conventional bias compensation in image space or object space.

Given initial RPCs (provided by the supplier or generated by users via the terrain-independent approach), a correction vector of the RPCs can be calculated from formula (9) using additional GCPs

$$\begin{aligned} \mathbf{L} &= \mathbf{A}(\mathbf{x}^0 + \Delta\mathbf{x}) + \mathbf{V} \\ \text{or} \quad \mathbf{L}' &= \mathbf{A}\Delta\mathbf{x} + \mathbf{V} \end{aligned} \tag{9}$$

where

$$\begin{aligned} &\mathbf{L}' = \mathbf{L} - \mathbf{A}\mathbf{x}^0; \\ &\mathbf{x}^0 = [a_0^0, \ldots, a_{19}^0, b_1^0, \ldots, b_{19}^0, \\ &\qquad c_0^0, \ldots, c_{19}^0, d_1^0, \ldots, d_{19}^0]^\top \text{ initial value of RPCs;} \\ &\Delta\mathbf{x} = [a_0^\delta, \ldots, a_{19}^\delta, b_1^\delta, \ldots, b_{19}^\delta, \\ &\qquad c_0^\delta, \ldots, c_{19}^\delta, d_1^\delta, \ldots, d_{19}^\delta]^\top \text{ correction vector of RPCs;} \end{aligned}$$

$\mathbf{L}, \mathbf{A}, \mathbf{V}$ are the same as those in Section III-A, and $\mathbf{x}^0 + \Delta\mathbf{x}$ denotes the corrected RPCs.

In formula (9), b_0 and d_0 of the initial RPCs are supposed to be 1. However, in the case of OrbView-3, etc., b_0 and d_0 of the provided RPCs are not exactly equal to 1, and we suggest reforming the RPCs by dividing each line coefficient by b_0 and each sample coefficient by d_0 to yield a group of new RPCs, in which only 78 RPCs are not constant.

Then, the correction vector $\Delta\mathbf{x}$ can be estimated via a similar process as Procedure 1. Note that, by applying the ℓ_1-norm regularization, only a small number of GCPs (even a single GCP) are needed to obtain $\Delta\mathbf{x}$, which will be verified in Section IV.

Comparing to the conventional rigorous sensor model and terrain-independent RFM with bias compensation in image space or in object space, superiorities of the direct RPC refining approach can be summarized as follows.

1) Users do not necessary have knowledge about the rigorous sensor model.
2) Less GCPs are needed than rigorous sensor model correction.

TABLE I
INFORMATION OF THE IMAGES USED IN THE EXPERIMENTS

Test name		Source image	District	GSD (m)	Coverage area (km^2)	Elevation range (m)	Reference data
Terrain-dependent Case	Test 1	HJ-1 level 2	Northeast of China	30	185×185	$0 \sim 2650$	Landsat-5
	Test 2	Landsat-5 L2	Xinjiang, China	30	185×185	$600 \sim 4000$	Landsat-5
Terrain-independent Case	Test 1	ALOS AVNIR2 1B2	Heilongjiang, China	10	70×70	$10 \sim 1061$	ALOS PRISM
	Test 2	IKONOS-2	Hobart, Australia	1	11×11	-3 $\sim$ 1263	GPS
Comprehensive Experiment		SPOT-5 HRG 1A	Tianjin, China	2.5	60×60	-50 $\sim$ 200	Quickbird

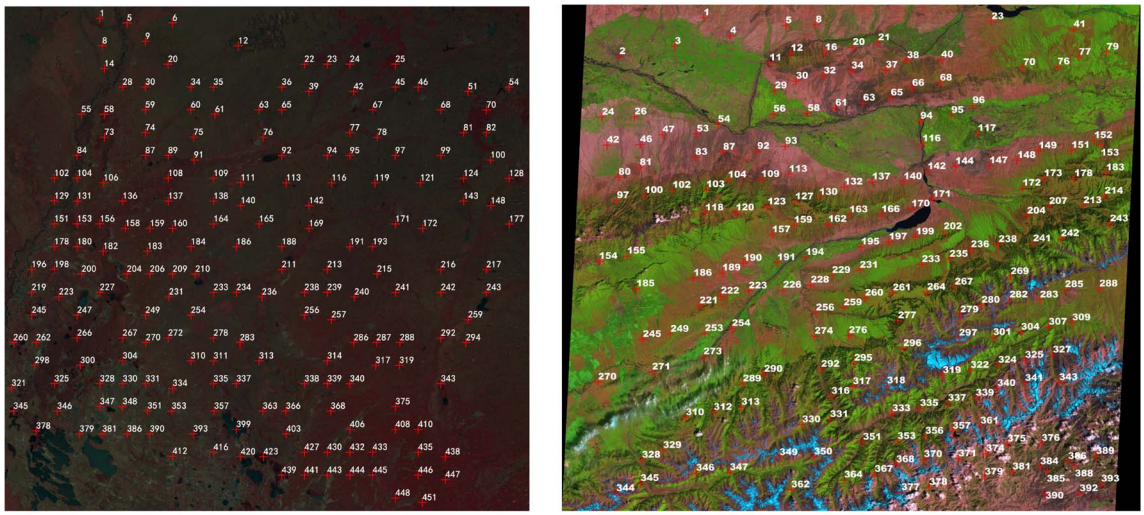

(a) (b)

Fig. 1. Distribution of 200 tie points in two tests. (a) HJ-1 image in test 1. (b) Landsat-5 image in test 2.

3) The form of the model is invariant for different numbers of GCPs, while the regular bias compensation in image space or object space has to choose simpler (with less unknowns) models when very few GCPs are used.
4) Higher accuracy can be achieved when more additional GCPs are available.

IV. EXPERIMENTAL VALIDATION

The experiments are conducted from three aspects: a robust RPC estimation in the terrain-dependent case, an RPC correction in the terrain-independent case, and a comprehensive study of the terrain-dependent model, terrain-independent model, and rigorous sensor model. Table I shows the general information of the test images used in these experiments.

As many approaches are involved in this section, the following abbreviations will be used to make the statement concise and clear:

1) OLS: ordinary least squares;
2) RE: ridge estimation;
3) L1LS: ℓ_1-norm-regularized least squares;
4) BSIC: bias compensation in image space;
5) NRBOS: directly correcting the simplified RFM based on NRBOS [16];
6) PCI: rigorous sensor model of PCI Geomatics 2013;
7) TD-L1LS: terrain-dependent approach based on ℓ_1-norm-regularized least squares;
8) TID-L1LS: directly correcting terrain-independent RPCs based on ℓ_1-norm-regularized least squares.

A. Robust RPC Estimation in Terrain-Dependent Case

To verify the proposed approach, two sets of images are tested in this section.

Test 1: HJ-1 Image: A scene of HJ-1 level 2 image in the northeast of China, whose spatial resolution is 30 m, is used in this test. The original coverage area of the HJ-1 imagery is 360×360 km^2, and we clip this image into 185×185 km^2 to match the coverage area of a Landsat-5 image, which is applied as the georeference of the HJ-1 image. The elevation range is from sea level to 2650 m. By using the automatic matching module of RSAutoCorrSys software, 589 tie points are found from the Landsat-5 image and HJ-1 image.

Test 2: Landsat-5 Image: A scene of Landsat-5 TM L2 image (spatial resolution is 30 m) captured in July 2009 was used in this test. The image is in Aksu district, Xinjiang, China, and the elevation range is from 600 to 4000 m, including some high mountains. Another scene of Landsat-5 TM L4 image

TABLE II
ACCURACY REPORT OF TEST 1

no. of GCPs (ICPs)	Method	GCPs accuracy (pixels)				ICPs accuracy (pixels)			
		RMSEs		MAX		RMSEs		MAX	
		Column	Row	Column	Row	Column	Row	Column	Row
80 (120)	L1LS	**0.34**	**0.37**	**-0.86**	**-1.03**	**0.34**	**0.37**	**-0.98**	**0.98**
	RE	0.25	0.28	-0.85	-0.80	0.52	0.43	-2.51	-1.21
	OLS	2.60	1.52	22.31	10.73	1.16	5.80	-7.26	-40.40
40 (160)	L1LS	**0.36**	**0.39**	**0.88**	**-1.03**	**0.40**	**0.42**	**1.13**	**1.10**
	RE	0.20	0.22	-0.60	-0.68	1.43	0.60	-14.06	2.74
	OLS	0.17	0.68	0.71	3.93	4.32	8.56	-46.17	-74.05
10 (190)	L1LS	**0.24**	**0.36**	**-0.53**	**0.92**	**0.64**	**0.56**	**-1.56**	**1.27**

TABLE III
ACCURACY REPORT OF TEST 2

no. of GCPs (ICPs)	Method	GCPs accuracy / pixels				ICPs accuracy / pixels			
		RMSEs		MAX		RMSEs		MAX	
		Column	Row	Column	Row	Column	Row	Column	Row
80 (120)	L1LS	**0.31**	**0.32**	**0.75**	**1.18**	**0.42**	**0.38**	**-1.04**	**-0.95**
	RE	0.27	0.30	-0.76	1.19	0.45	0.39	1.49	1.04
	OLS	1.16	1.19	6.90	9.48	106.30	2.57	-1161.23	25.42
40 (160)	L1LS	**0.23**	**0.18**	**-0.64**	**0.35**	**0.46**	**0.43**	**-1.17**	**1.45**
	RE	0.21	0.16	-0.57	0.35	0.93	0.75	-6.90	5.33
	OLS	0.33	3.85	1.84	24.30	3.34	2.38	27.93	22.32
10 (190)	L1LS	**0.17**	**0.28**	**-0.38**	**-0.48**	**0.45**	**0.55**	**-1.06**	**1.8**

(orthoproduct) in the same place captured in August 2007 was used as the reference image. Here, 393 tie points from the two images were found by the automatic matching module of RSAutoCorrSys software.

For each test, 200 well-distributed tie points are selected from the automatically matched tie points (as shown in Fig. 1). Then, 10, 40, and 80 tie points are evenly selected as GCPs, and the remaining (190, 160, and 120) tie points are used as independent check-points (ICPs). Three methods, including OLS, RE, and ℓ_1-*norm-regularized least squares* (L1LS), are used to estimate RPCs, respectively. The accuracy reports are shown as Tables II and III, containing the root-mean-square errors (rmses) and maximum residuals of GCPs and ICPs. For the 80-GCP and 40-GCP cases, the results of all three methods are listed, while the results of OLS and RE are omitted for the 10-GCP case because they do not provide reasonable results when the normal matrix is rank deficient. In the two tests, the regularization parameter λ is set to 10^{-4}.

According to Tables II and III, some points can be drawn.

1) The problem of solving RPCs is seriously ill-posed, and OLS yields unstable results in both tests.
2) ℓ_2-norm-regularized least squares (ridge estimation) improves the solution of OLS. When the number of GCPs is much greater than 39 (80-GCP case), ridge estimation provides reliable results. When the number of GCPs is not much greater than 39 (40-GCP case), however, ridge estimation performs badly at ICPs. Despite the high fitting accuracy at GCPs, the estimated model can be oscillatory between exact-fit values. That is why the accuracy of ICPs is much worse than that of GCPs, especially for some oscillatory position (as the maximum residuals indicate). In this sense, much more than 39 GCPs are required to yield reliable RPCs when ridge estimation is applied.
3) ℓ_1-norm-regularized least squares has much better performance at ICPs than ridge estimation. Although ℓ_1-norm-regularized least squares does not provide as good fits as ridge estimation at GCPs, it guarantees the accuracy of ICPs. L1LS automatically omits some coefficients which might make the model unstable.
4) L1LS performs robustly when different numbers of GCPs are used. Even in the 10-GCP case, this method provides practical results (the maximum residuals of ICPs are less than 2 pixels). In this sense, it is possible to perform accurate orthocorrection without knowing the rigorous sensor model using a small amount of GCPs.

B. RPC Correction in Terrain-Independent Case

In this section, two tests were carried out using ALOS AVNIR2 1B2 image and IKONOS image, respectively.

Test 1: ALOS AVNIR2 1B2 Image: A scene of ALOS AVNIR2 1B2 image (spatial resolution is 10 m) in Heilongjiang district of China, whose elevation range is from 10 to 1016 m,

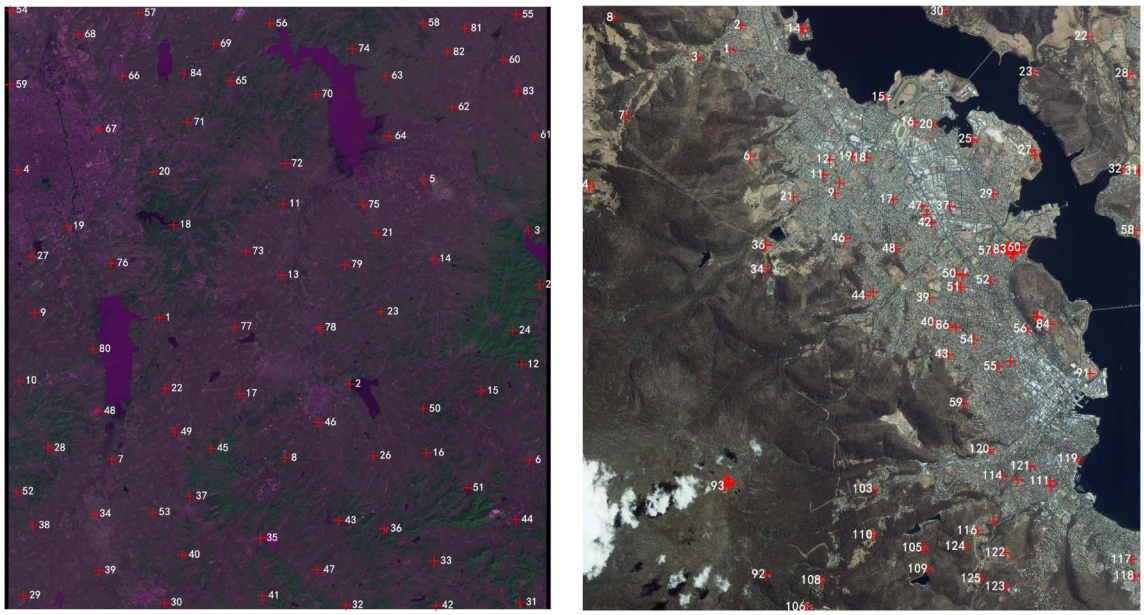

(a) (b)

Fig. 2. Distribution of the tie points in two tests. (a) ALOS image in test 1. (b) IKONOS image in test 2.

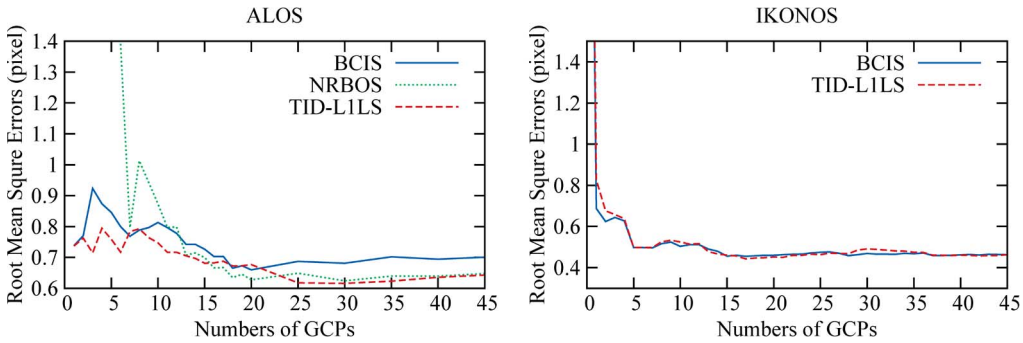

Fig. 3. Accuracy comparison of different methods using different numbers of GCPs. BCIS denotes "bias compensation in image space," NRBOS denotes "directly correcting the simplified RFM based on NRBOS," and TID-L1LS denotes "directly correcting terrain-independent RPCs based on ℓ_1-norm-regularized least squares."

was used to carry out comparative tests. The orthorectified ALOS PRISM image, whose rmse is about 2.5 m, was used as reference image. The terrain-independent RPCs used in the tests are provided by the image supplier. Here, 84 GCPs [see Fig. 2(a)] were collected in the range of the image, and the height of the GCPs was obtained from ASTER GDEM Version 2. The GCPs meet the accuracy requirements of at least three times more precise than the target specification for the ortho [37]. Different numbers of points (varying from 1 to 45) were selected from the 84 points as GCPs, while the rest were treated as check-points. Three approaches, including the *bias compensation in image space* (BCIS), *directly correcting the simplified RFM based on NRBOS* [16] (NRBOS), and *directly correcting terrain-independent RPCs based on ℓ_1-norm-regularized least squares* (TID-L1LS), were used to correct the RPCs. The simplified RFM was an approximate model statistically obtained from the coefficient selection tests of 38 ALOS AVNIR2 1B2 images, which contains five sample coefficients and six line coefficients, and at least six GCPs are needed to perform NRBOS.

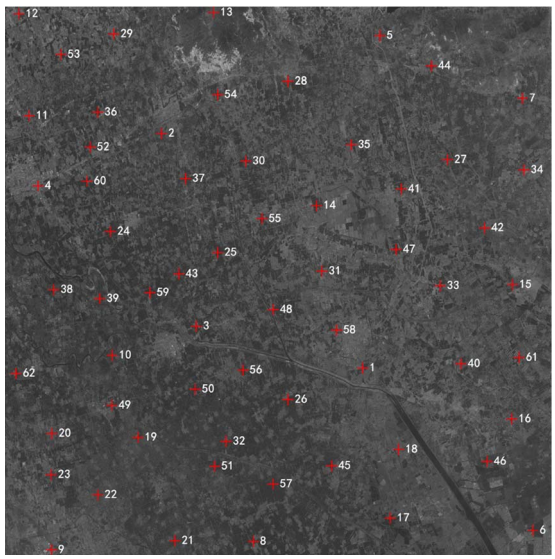

Fig. 4. Distribution of the 62 GCPs of the SPOT-5 image.

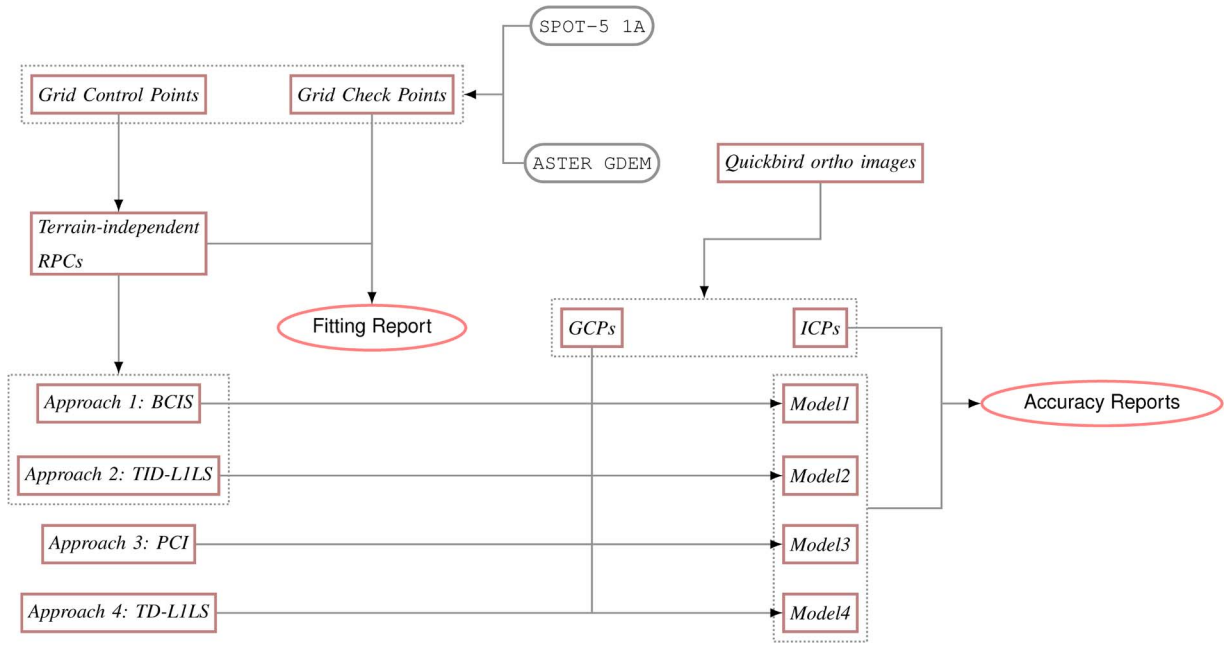

Fig. 5. Outline of the comprehensive experiment.

Test 2: IKONOS-2 Image: A scene of IKONOS-2 image (spatial resolution is 1 m) captured in February 2003 was used in this test. The image is in Hobart, Australia, and the elevation range is from -3 to 1263 m. Here, 125 GPS-surveyed GCPs [see Fig. 2(b)] were available in the range of this image. Different numbers of points (varying from 1 to 45) were selected from the 125 points as GCPs, while the rest were treated as check-points. The *bias compensation in image space* (BCIS) and *directly correcting terrain-independent RPCs based on ℓ_1-norm-regularized least squares* (TID-L1LS) were used to correct the terrain-independent RPCs, respectively.

For BCIS, translation-model is applied when a single additional GCP is used, shift-model is applied when two additional GCPs are used, and affine-model is applied when no less than three additional GCPs are available. In contrast, TID-L1LS can be applied without modification for different numbers of additional GCPs. In the TID-L1LS tests of the two images, the regularization parameter λ is set to 10^{-4}. Fig. 3 shows the rmses of the check-points using different methods and different numbers of GCPs.

From Fig. 3, the following can be found that.

1) Both BCIS and TID-L1LS can be applied to refine the RFM with a single or quite a few additional GCPs, and the accuracy of the refined RFMs is practical.
2) When only a few GCPs are used in the test of the ALOS image, the results of TID-L1LS are more stable than those of BCIS and NRBOS. For BCIS, the affine-model is used when the number of GCPs is greater than 2, but the superiority of the affine-model to the shift-model does not show until the number of GCPs is greater than 6. NRBOS requires at least six GCPs, and the accuracy vacillates when the number of GCPs is less than 10.
3) In the test of the ALOS image, NRBOS and TID-L1LS achieve higher accuracy than BCIS when GCPs are sufficient. BCIS models the biases of RPCs based on the assumption that the systematic errors of the RPCs only result from invariant biases of position and attitude data throughout the scene, while NRBOS and TID-L1LS do not make this assumption. Consequently, it is possible for NRBOS and TID-L1LS to correct the coefficients to a greater extent than that can be done by BCIS, therefore obtaining higher accuracy when sufficient GCPs are used.
4) In the test of the IKONOS-2 image, BCIS and TID-L1LS achieve comparable accuracy. After precise onboard geometric calibration, the elements of the interior orientation of IKONOS have been determined to superb accuracy, and many effects on exterior orientation error are negligible or completely correlated with other effects. As a result, only a few parameters are required to effectively model the sensor errors [10], [38]. Moreover, this scene of the IKONOS image is not of long strips (11 km $\times$ 11 km), and affine transformation compensation in image space is accurate enough to model the sensor errors. In this case, the superiority of TID-L1LS in correcting terrain-independent RPCs is not obvious.

TABLE IV
FITTING ACCURACY OF TERRAIN-INDEPENDENT RPCS

	RMSEs / pixel		MAX / pixel	
	Column	Row	Column	Row
Control Grid Points	0.121	0.362	-0.321	1.045
Check Grid Points	0.121	0.373	-0.347	1.469

C. Comprehensive Experiment

In this experiment, a scene of SPOT-5 HRG 1A image (spatial resolution is 2.5 m) in Tianjin district of China, whose

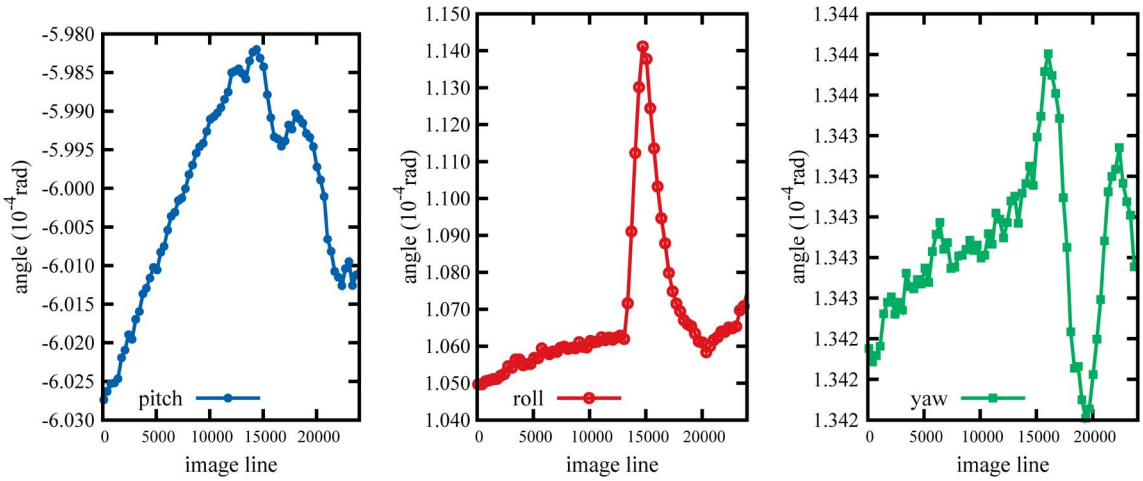

Fig. 6. Attitude angles of the lines in the SPOT-5 image.

elevation range is from −50 to 200 m, was used as test image, and orthorectified QuickBird images, whose rmse is about 0.6 m, were used as reference data. To calculate and check the terrain-independent RPCs, $5 \times 15 \times 15$ 3-D control grid points and $10 \times 30 \times 30$ 3-D check grid points were established according to the rigorous sensor model [39]. Moreover, to refine the terrain-independent RPCs, 62 GCPs (see Fig. 4) were collected, referencing the orthoimages of QuickBird, and the height of GCPs was obtained from ASTER GDEM Version 2. The workflow of the experiment is shown in Fig. 5. The regularization parameter λ is set to 10^{-5} in the tests.

First, the 3-D control grid points were used to calculate the terrain-independent RPCs, and the 3-D check grid points were used to check the fitting accuracy. Note that the RPCs were estimated using L1LS, and similar results can be obtained by using ridge estimation. Table IV shows the accuracy, including rmses and maximum residuals of the control grid points and check grid points.

From Table IV, one can see that the calculated terrain-independent RFM approximates the rigorous sensor model better than 0.4 pixels in rmses. Nevertheless, the residuals in line (raw) direction of some of the virtual control grid points and check grid points are greater than 1 pixel. The great residuals may result from the instability of the satellite attitude when the image was acquired. Fig. 6 shows the attitude angles (pitch, roll, and yaw) of the lines in the SPOT-5 image, and one can observe sudden changes of roll angle and yaw angle near the range of 15 000 lines and 20 000 lines, respectively. Although the rigorous sensor model can model the time-dependent imaging geometry [40], it is reasonable that the RFM failed to fit the rigorous sensor model within subpixels. However, the estimated RFM can generally be applied to replace the rigorous sensor model with error less than 2 pixels.

Second, different numbers of GCPs (from 0 to 40) were selected from all of the 62 GCPs, and the rest were treated as ICPs. Then, for each pair of GCPs and ICPs, four approaches, including *bias compensation in image space* (BCIS), *directly correcting terrain-independent RPCs based on ℓ_1-norm-regularized least squares* (TID-L1LS), *rigorous sensor model of PCI Geomatics 2013* (PCI), and *terrain-dependent approach based on ℓ_1-norm-regularized least squares* (TD-L1LS), were applied to estimate the final imaging models with the help of GCPs. Then, ICPs were used to check the accuracy of the final imaging models. The first two approaches utilized the GCPs to correct the calculated terrain-independent RPCs, and the third approach utilized the GCPs to correct the rigorous sensor model, while the last approach directly estimated the RPCs from GCPs without knowing the terrain-independent RPCs or rigorous sensor model. Note that the translation-model, shift-model, and affine-model were used by BCIS for different numbers of GCPs, just as what was done in Section IV-B. The rmses and maximum residuals of four approaches are shown in Fig. 7.

The results of the comprehensive experiment can be summarized as follows.

1) Without any GCPs, the rmse and maximum residual of the calculated terrain-independent RFM in ICPs are 9.62 and 12.14 pixels, while those of the initial rigorous sensor model in PCI Geomatics 2013 are 8.59 and 10.72 pixels. The difference in accuracy between the two models may result from the fitting error of the terrain-independent RFM (about 1.5 pixels).
2) When a single GCP was used, TID-L1LS and BCIS achieved comparable accuracy at ICPs (rmse is about 1.7 pixels, and maximum residual is about 3.7 pixels), and the accuracy generally improves as the number of GCPs increases. However, the terrain-dependent approach and the rigorous sensor model in PCI Geomatics 2013 cannot provide reasonable results with so few GCPs.
3) The rigorous sensor model in PCI Geomatics 2013 requires at least six GCPs to yield reasonable results. However, when more than six GCPs are utilized, the corrected rigorous sensor model becomes quite accurate and stable.
4) For TID-L1LS, when more than six GCPs were used, both the rmses and maximum residuals are comparable with those of the rigorous sensor model.
5) For BCIS, a small amount of GCPs can also be applied to correct the calculated terrain-independent RPCs. However, the maximum residuals are a bit greater than those

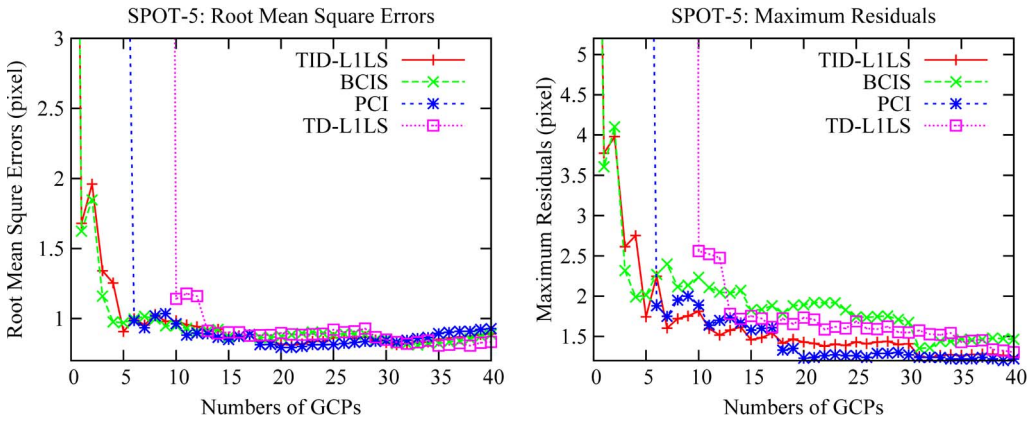

Fig. 7. Accuracy comparison of different methods using different numbers of GCPs.

of TID-L1LS and rigorous sensor model when sufficient GCPs are applied.

6) Owning to the ℓ_1-norm regularization, it is possible for the terrain-dependent approach to calculate the RPCs with less than 39 GCPs. However, the results of TD-L1LS are oscillatory and not reasonable until more than 13 GCPs are used (rmses and maximum residuals are around 0.9 and 1.8 pixels). When more than 13 GCPs are utilized, the results of TD-L1LS become quite stable, the rmses are comparable with those of TID-L1LS and rigorous sensor model, and the maximum residuals are less than those of BCIS.

D. Selection of Parameter λ and Some Discussion

1) Sensitivity of Parameter λ: According to Procedure 1, ℓ_1-norm-regularized least squares (L1LS) involves an optimal regularization parameter λ, and in the previous experiments, a constant value (10^{-4}) was used to assess the robustness of the proposed method. Experientially, $\lambda = 10^{-4}$ commonly performs well for the tested remotely sensed images. However, it is not always the optimal one to yield the best results. In this section, a range of values (10^{-7} to 10^{-3}) was applied to λ to discuss its impact on the performance. All of the data in Sections IV-A, IV-B, and IV-C were used in this experiment, and 40 GCPs were selected for each image, while the rest were treated as check-points. The rmse and maximum residual of the check-points were used to evaluate the performance of the L1LS method (as shown in Fig. 8). For HJ-1 level 2 and Landsat-5 L2, terrain-independent RFMs were not utilized; therefore, only the results of TD-L1LS were included. For the other three images, both of the results of TD-L1LS and TID-L1LS were included.

According to Fig. 8, in all of the tests, the optimal λ can be found around the range $10^{-5} \sim 10^{-4}$. Concretely, for most of the TID-L1LS cases (except for SPOT-5) and TD-L1LS cases of Landsat-5 TM L2, HJ-1 level 2, and ALOS AVNIR2 1B2, the optimal λ is around 10^{-4}; for the TD-L1LS case of IKONOS-2 and both TD-L1LS case and TID-L1LS case of SPOT-5 HRG 1A, the optimal λ is around 10^{-5}. Note that the empirical values that we used in the previous tests are not the optimal ones, and the technique to search the optimal λ is not included in this work. One can also apply GCV to search λ, but GCV frequently yields bad results according to our tests. The authors recommend to use empirical values as one can commonly specify the range of the optimal λ's with the help of the prior knowledge about the problems.

Essentially, the impact of λ on the accuracy of the check-points is caused by the output RPCs. As ℓ_1-norm-regularized least squares commonly yields sparse results in which a number of elements are shrunk to zero, different λ's may result in RPCs of different numbers of nonzero elements. Generally, a larger λ is expected to yield sparser RPCs (less nonzero coefficients). Take the SPOT-5 image as an example, 30 nonzero coefficients $(a_0 \sim a_2, a_4, a_7, a_8, a_{14}, b_0, b_4, b_7 \sim b_9, b_{11}, b_{14}, c_0 \sim c_4, c_{11}, c_{12}, c_{15}, c_{19}, d_0 \sim d_2, d_4, d_{11}, d_{12}, d_{14})$ were obtained if λ was set to 10^{-5}, while 14 nonzero coefficients $(a_0 \sim a_2, a_4, a_7, b_0, c_0 \sim c_2, c_4, c_{19}, d_0 \sim d_2)$ were obtained if λ was set to 10^{-3}. Obviously, most of the remaining nonzero coefficients are the low-order items of the original RFM, while most of the high-order items of the original RFM, which usually result in collinearity and instability, are shrunk to zeros. However, some of the remaining high-order items (such as $a_{14}, b_{11}, b_{14}, c_{11}, c_{12}, c_{15}, c_{19}, d_{11}, d_{12}, d_{14}$) are also important to form a precise sensor model as they can proximate the significant high-frequency dynamic changes in sensor acceleration and orientation, etc. [3]

Not only the parameter λ affects the number of remaining RPCs, the distortion complexity of the image and the number of GCPs also have an impact on the sparsity of the output model. Generally, a more complicated distortion of the image will result in more nonzero elements in the estimated RPCs, as the RFM needs more parameters to correct the errors of the sensor. On the other hand, the amount of GCPs greatly limits the number of output nonzero coefficients only when the number of GCPs is few, and the number of output nonzero coefficients does not necessarily relate to the number of GCPs if the GCPs are sufficient.

Examining the results in Fig. 8 again, the following points can be drawn.

1) In TID-L1LS cases, most of the sensor's errors have been modeled by the terrain-independent RFM, and the

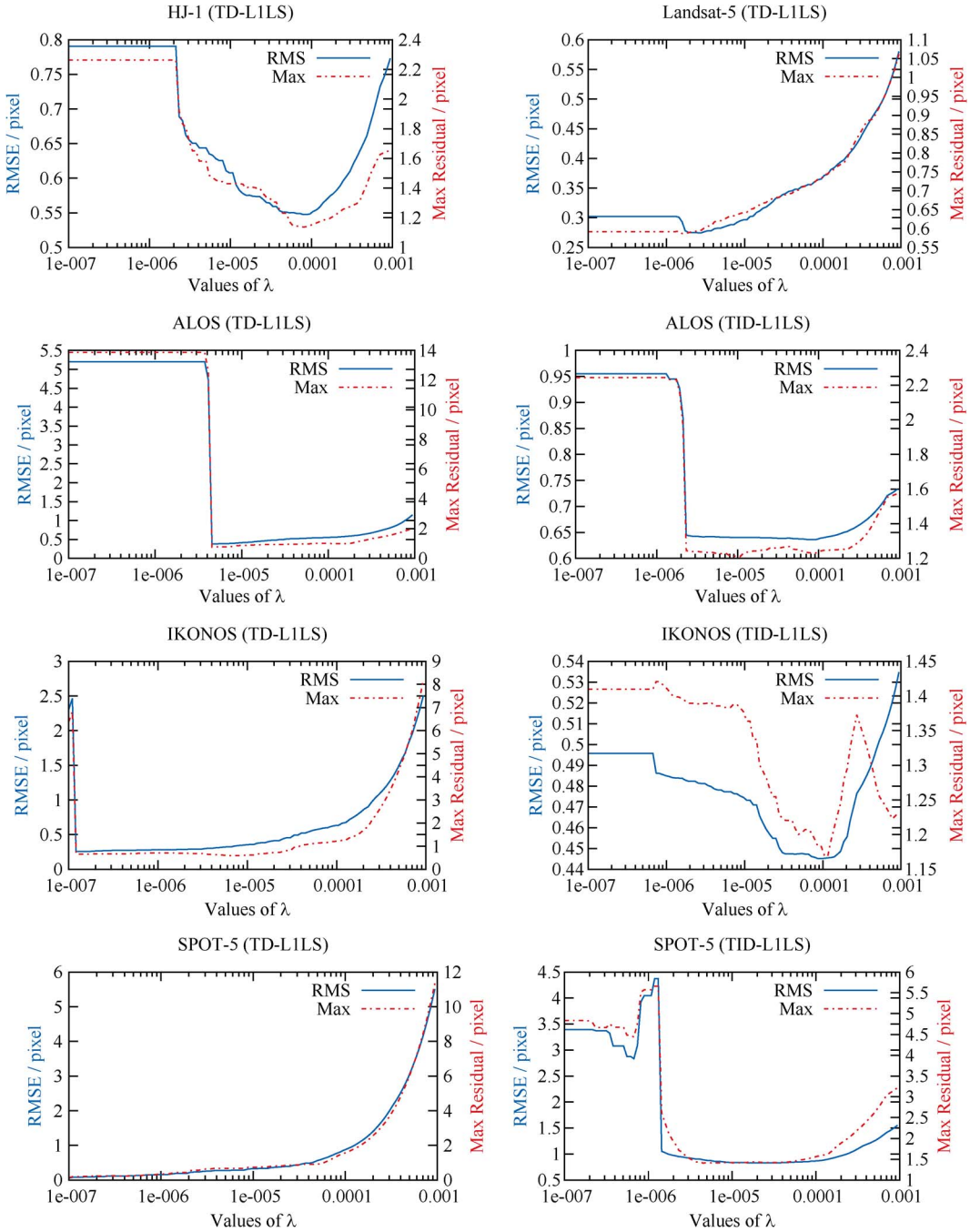

Fig. 8. Accuracy of check-points versus value of λ.

refinement requires much fewer parameters to correct the remaining errors; thus, a larger λ is needed to yield a sparser model.

2) In the TID-L1LS case of SPOT-5, the fitting accuracy of the terrain-independent RFM is around 1.5 pixels, and the refinement needs more parameters to precisely model the error. Thus, the optimal λ is around 10^{-5}.
3) Commonly, the refinement of the terrain-independent RFM and the estimation of the terrain-dependent RFM of the image products of level-2 (systematically geometric corrected) are suggested to apply a λ around 10^{-4}, and the estimation of the terrain-dependent RFM of the image products of level-1 (without systematical geometric correction) is suggested to apply a λ around 10^{-5}.

2) More Discussions: To illustrate the impact of the number of GCPs and distortion complexity of images on the number of output nonzero coefficients, five TD-L1LS tests of images in Table I were carried out, in which 3–60 GCPs were used for the five images, and the rest of the available GCPs were applied as check-points. Note that, in the tests of IKONOS and SPOT-5, λ was set to 10^{-5} and λ was set to 10^{-4} in the other tests. Fig. 9 shows the number of nonzero coefficients in the output RPCs and the rmses of the check-points.

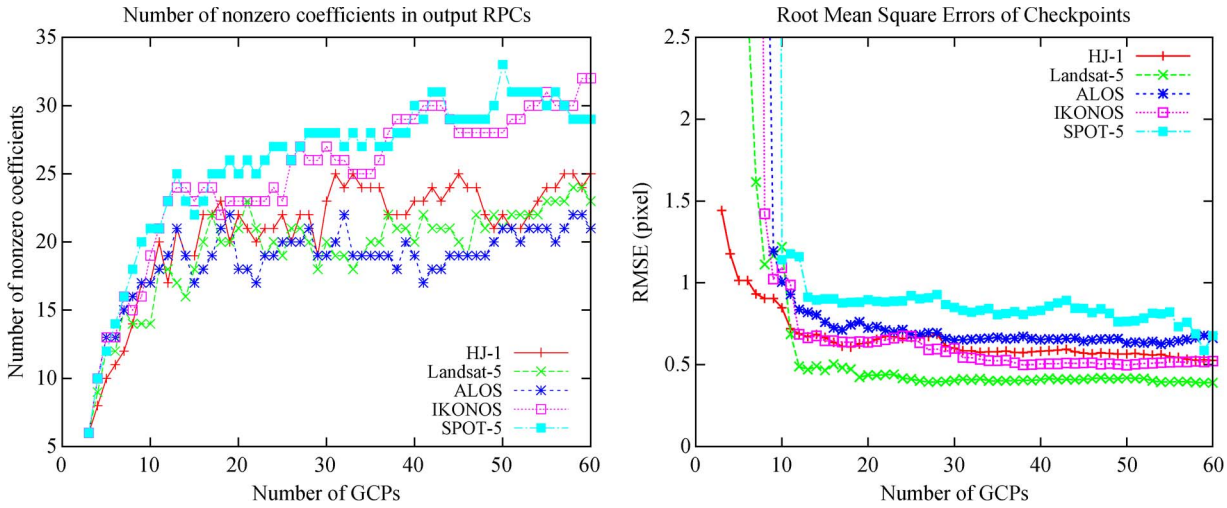

Fig. 9. Number of nonzero coefficients and rmses of the check-points versus the number of GCPs.

From Fig. 9, it can be found that, when the number of GCPs is few (fewer than ten), the number of output nonzero coefficients is greatly limited by the number of GCPs, and the accuracy of the check-points is bad. When GCPs are adequate (about 20 GCPs), the number of output nonzero coefficients may not increase with the number of GCPs observably, as well as the accuracy of the check-points. Although the number of nonzero coefficients varies in a small range, it stabilizes around a value when GCPs are adequate, which differs from one image to another. For HJ-1, Landsat-5, and ALOS, the value is about 20, while for IKONOS and SPOT-5, it is about 30.

E. Some Conclusion

According to the aforementioned experimental results, we can conclude the following.

1) The rigorous sensor model is the most related to the imaging process of the remotely sensed images and can obtain a very high accuracy with several GCPs. Generally, correction for the systematic error of the rigorous sensor model is performed by amending the orientation parameters, e.g., position and attitude data, which are highly independent. Thus, at least three GCPs are required to estimate all of the correction values of six orientation parameters, and more GCPs (more than five) are commonly needed to make the estimation reliable. Moreover, the rigorous sensor model requires detailed knowledge about the sensor and platform and can be very complicated and computationally intensive, especially for the inverse model [39].
2) Bias compensation in image space can refine the calculated terrain-independent RPCs with a small amount of (or without) GCPs. However, the accuracy of affine transformation in image space is limited as the bias of the terrain-independent RPCs or the original rigorous sensor model may be more complicated than simple affine distortion in image space for the SPOT-5 HRG 1A image.
3) Directly correcting the terrain-independent RPCs based on ℓ_1-norm regularization has a similar performance of bias compensation in image space when no GCP or several GCPs are used. When more GCPs are available (more than six GCPs), it provides more accurate models than bias compensation in image space and can reach comparable accuracy of the rigorous sensor model. Unlike bias compensation in image space, this approach is not limited to narrow field of view. Additionally, comparing to the rigorous sensor model, it is much easier and efficient for naive users to perform direct correction with additional GCPs to obtain precision products if they are provided with the calculated terrain-independent RPCs.
4) Terrain-dependent approach based on ℓ_1-norm regularization can be used to calculate RPCs when the number of GCPs is less than 39, which is the minimum number of GCP requirement of the conventional approaches (e.g., OLS, ridge estimation, etc.). Although it is possible for this approach to estimate terrain-dependent RPCs with a few GCPs, too few GCPs may make the calculated RFM unstable. However, the terrain-dependent RFM will become more stable when more GCPs are used. Note that the minimum number of GCPs which makes the terrain-dependent RFM stable differs from different types of images due to the different complexities of distortion. For example, in the aforementioned experiments, it can be seen that no less than 13 GCPs are required to get a stable terrain-dependent RFM for this SPOT-5 HRG 1A image. However, for Landsat-5 TM L2 images (see Section IV-A), a stable terrain-dependent RFM can be obtained with less than ten GCPs.
5) Although the terrain-dependent approach based on ℓ_1-norm regularization requires more GCPs to obtain a stable model than bias compensation in image space and directly correcting the terrain-independent RPCs based on ℓ_1-norm regularization, it does not require any prior knowledge of the rigorous sensor model or terrain-independent RPCs. Moreover, when sufficient GCPs are used, the terrain-dependent RFM can be more accurate than the affine-corrected terrain-independent RFM.

V. Conclusion and Suggestions

In this paper, a novel approach using ℓ_1-norm-regularized least squares (L1LS) has been proposed to estimate RPCs, and it can benefit both the terrain-dependent RFM and the terrain-independent RFM.

1) For the terrain-dependent RFM case, the proposed approach can be applied to estimate parsimonious and robust RPCs with less observation data and get similar accuracy as rigorous sensor model, while the conventional approaches require more observations, and the solution may be unstable due to the strong correlation between the coefficients. In other words, it becomes possible to perform accurate orthocorrection without knowing the rigorous sensor model using a small amount of GCPs.
2) For the terrain-independent RFM case, the proposed approach can also be applied to directly correct the terrain-independent RPCs with additional GCPs. For conventional compensation in image space or object space, the translation-model, shift-model, or affine-model needs to be applied when different numbers of GCPs are used. In contrast, the proposed direct correction approach can be adopted without modification for different numbers of GCPs. When a single or several GCPs are used, the results of the proposed approach are comparable with those of bias compensation in image space; when more GCPs are available, the proposed approach shows better potential to correct the terrain-independent RPCs and can reach better accuracy (comparable with that of the rigorous sensor model) than conventional bias compensation in image space.

However, the regularization parameter is empirically selected, and it is not the optimal one sometimes. Our future work will be devoted to automatically find the optimal regularization parameter for different images and applications.

Acknowledgment

The authors would like to thank Space Imaging LLC for making a set of IKONOS imagery available for research and also C. Fraser's research group at the University of Melbourne for providing the surveyed ground control points.

References

[1] D. Poli and T. Toutin, "Review of developments in geometric modeling for high resolution satellite pushbroom sensors," *Photogramm. Rec.*, vol. 27, no. 137, pp. 58–73, Mar. 2012.
[2] J. Grodecki, "IKONOS stereo feature extraction-RPC approach," in *Proc. ASPRS Annu. Conf.*, St. Louis, MO, USA, 2001, pp. 23–27.
[3] C. S. Fraser, G. Dial, and J. Grodecki, "Sensor orientation via RPCs," *ISPRS J. Photogramm. Remote Sens.*, vol. 60, no. 3, pp. 182–194, May 2006.
[4] OGC, "Consortium. The OpenGis abstract specification," 1999.
[5] Y. Hu and C. V. Tao, "Updating solutions of the rational function model using additional control information," *Photogramm. Eng. Remote Sens.*, vol. 68, no. 7, pp. 715–724, 2002.
[6] C. S. Fraser and H. B. Hanley, "Bias-compensated RPCs for sensor orientation of high-resolution satellite imagery," *Photogramm. Eng. Remote Sens.*, vol. 71, no. 8, pp. 909–915, Aug. 2005.
[7] Q. Zhang, Z. Li, H. Pan, Q. Qiang, and L. Zhai, "Orientation of spaceborne SAR stereo pairs employing the RPC adjustment model," *IEEE Trans. Geosci. Remote Sens.*, vol. 49, no. 7, pp. 2782–2792, Jul. 2011.
[8] Z. Xiong and Y. Zhang, "Bundle adjustment with rational polynomial camera models based on generic method," *IEEE Trans. Geosci. Remote Sens.*, vol. 49, no. 1, pp. 190–202, Jan. 2011.
[9] T. A. Teo, L. C. Chen, C. L. Liu, Y. C. Tung, and W. Y. Wu, "DEM-aided block adjustment for satellite images with weak convergence geometry," *IEEE Trans. Geosci. Remote Sens.*, vol. 48, no. 4, pp. 1907–1918, Apr. 2010.
[10] J. Grodecki and G. Dial, "Block adjustment of high-resolution satellite images described by rational polynomials," *Photogramm. Eng. Remote Sens.*, vol. 69, no. 1, pp. 59–68, 2003.
[11] C. Tao and Y. Hu, "A comprehensive study of the rational function model for photogrammetric processing," *Photogramm. Eng. Remote Sens.*, vol. 67, no. 12, pp. 1347–1357, 2001.
[12] T. Poggio, V. Torre, and C. Koch, "Computational vision and regularization theory," *Nature*, vol. 317, no. 26, pp. 314–319, Sep. 1985.
[13] N. Draper, H. Smith, and E. Pownell, *Applied Regression Analysis*. New York, NY, USA: Wiley, 1966, vol. 3.
[14] X. Yuan and J. Cao, "An optimized method for selecting rational polynomial coefficients based on multicollinearity analysis," *Geom. Inf. Sci. Wuhan Univ.*, vol. 36, no. 6, pp. 664–669, 2011.
[15] Y. Zhang, Y. Lu, L. Wang, and X. Huang, "A new approach on optimization of the rational function model of high-resolution satellite imagery," *IEEE Trans. Geosci. Remote Sens.*, vol. 50, no. 7, pp. 2758–2764, Jul. 2012.
[16] T. Long, W. Jiao, and G. He, "Nested regression based optimal selection (NRBOS) of rational polynomial coefficients," *Photogramm. Eng. Remote Sens.*, vol. 80, no. 3, pp. 261–269, 2014.
[17] E. J. Candes and T. Tao, "Decoding by linear programming," *IEEE Trans. Inf. Theory*, vol. 51, no. 12, pp. 4203–4215, Dec. 2005.
[18] D. L. Donoho, "Compressed sensing," *IEEE Trans. Inf. Theory*, vol. 52, no. 4, pp. 1289–1306, Apr. 2006.
[19] E. J. Candès and M. B. Wakin, "An introduction to compressive sampling," *IEEE Signal Process. Mag.*, vol. 25, no. 2, pp. 21–30, Mar. 2008.
[20] R. Tibshirani, "Regression shrinkage and selection via the Lasso," *J. Roy. Statist. Soc., Ser. B (Methodological)*, vol. 58, no. 1, pp. 267–288, 1996.
[21] S. S. Chen, D. L. Donoho, and M. A. Saunders, "Atomic decomposition by basis pursuit," *SIAM J. Sci. Comput.*, vol. 20, no. 1, pp. 33–61, 1998.
[22] B. Efron, T. Hastie, I. Johnstone, and R. Tibshirani, "Least angle regression," *Ann. Statist.*, vol. 32, no. 2, pp. 407–499, 2004.
[23] H. Zou and T. Hastie, "Regularization and variable selection via the elastic net," *J. R. Statist. Soc., Ser. B, Stat. Methodol.*, vol. 67, no. 2, pp. 301–320, Apr. 2005.
[24] K. Koh, S. J. Kim, and S. P. Boyd, "An interior-point method for large-scale-regularized logistic regression," *J. Mach. Learn. Res.*, vol. 8, pp. 1519–1555, Jul. 2007.
[25] M. Nikolova, "Description of the minimizers of least squares regularized with ℓ_0-norm. Uniqueness of the global minimizer," *SIAM J. Imag. Sci.*, vol. 6, no. 2, pp. 904–937, 2013.
[26] D. L. Donoho and M. Elad, "Optimally sparse representation in general (nonorthogonal) dictionaries via ℓ_1 minimization," *Proc. Nat. Acad. Sci.*, vol. 100, no. 5, pp. 2197–2202, 2003.
[27] R. Tibshirani, "Regression shrinkage and selection via the Lasso: A retrospective," *J. R. Statist. Soc., Ser. B, Stat. Methodol.*, vol. 73, no. 3, pp. 273–282, Jun. 2011.
[28] M. Schmidt, "Least squares optimization with L1-norm regularization," University of British Columbia, Vancouver, BC, USA, Project Rep., 2005.
[29] T. A. Davis, "Algorithm 832: UMFPACK V4. 3—An unsymmetric-pattern multifrontal method," *ACM Trans. Math. Softw.*, vol. 30, no. 2, pp. 196–199, 2004.
[30] M. R. Osborne, B. Presnell, and B. A. Turlach, "A new approach to variable selection in least squares problems," *IMA J. Numer. Anal.*, vol. 20, no. 3, pp. 389–403, 2000.
[31] J. Fan and R. Li, "Variable selection via nonconcave penalized likelihood and its oracle properties," *J. Amer. Statist. Assoc.*, vol. 96, no. 456, pp. 1348–1360, 2001.
[32] S. Perkins, K. Lacker, and J. Theiler, "Grafting: Fast, incremental feature selection by gradient descent in function space," *J. Mach. Learn. Res.*, vol. 3, pp. 1333–1356, 2003.
[33] T. Hastie, R. Tibshirani, and J. J. H. Friedman, *The Elements of Statistical Learning*. New York, NY, USA: Springer-Verlag, 2001, vol. 1.
[34] K. Sjöstrand, L. H. Clemmensen, R. Larsen, and B. Ersbøll, "Spasm: A MATLAB toolbox for sparse statistical modeling,"

Tech. Univ. Denmark, Lyngby, Denmark. [Online]. Available: http://www2.imm.dtu.dk/projects/spasm/references/spasm.pdf.
[35] Y. Hu, V. Tao, and A. Croitoru, "Understanding the rational function model: Methods and applications," *Int. Arch. Photogramm. Remote Sens.*, vol. 35, no. 4, pp. 663– 668, 2004.
[36] T. A. Teo, "Bias compensation in a rigorous sensor model and rational function model for high-resolution satellite images," *Photogramm. Eng. Remote Sens.*, vol. 77, no. 12, pp. 1211–1220, 2011.
[37] D. Kapnias, P. Milenov, and S. Kay, "Guidelines for best practice and quality checking of ortho imagery," Joint Res. Centre, Ispra, Italy, no. 3.0, 2008.
[38] G. Dial, H. Bowen, F. Gerlach, J. Grodecki, and R. Oleszczuk, "IKONOS satellite, imagery, and products," *Remote Sens. Environ.*, vol. 88, no. 1, pp. 23–36, 2003.
[39] S. Riazanoff, "SPOT 123-4-5 Geometry Handbook," GAEL Consultant, Champs-sur-Marne, France, Tech Rep. GAEL-P135-DOC-001, no. 1, 2004.
[40] H. Topan and D. Maktav, "Efficiency of orientation parameters on georeferencing accuracy of SPOT-5 HRG level-1A stereoimages," *IEEE Trans. Geosci. Remote Sens.*, vol. 52, no. 6, pp. 3683–3694, Jun. 2014.

Tengfei Long was born in Wuhan, China, in 1986. He received the B.Sc. degree in remote sensing from Wuhan University, Wuhan, in 2008 and the M.Sc. degree in cartography and geographic information systems from the Center for Earth Observation and Digital Earth, Chinese Academy of Sciences (CAS), Beijing, China, in 2011, where he has been working toward the Ph.D. degree in the Institute of Remote Sensing and Digital Earth since September 2013.

In 2011, he joined the Institute of Remote Sensing and Digital Earth, CAS, as a Research Assistant. His current research interests include spatial photogrammetry, image registration, land-cover change detection, and computer vision.

Weili Jiao received the B.Sc. degree in cartography from the Wuhan Technical University of Surveying and Mapping, Wuhan, China, in 1988 and the M.Sc. degree in geoinformatics from the International Institute for Aerospace Survey and Earth Sciences (ITC), Enschede, The Netherlands, in 1995.

She is currently a Professor with the Institute of Remote Sensing and Digital Earth (RADI), Chinese Academy of Sciences (CAS), Beijing, China. She has 26 years of expertise in the field of remote sensing image processing. Her current research interests include digital photogrammetry, image registration, spatial data uncertainty, land-cover mapping, and change detection.

Guojin He was born in Fujian, China, in 1968. He received the B.Sc. degree in geology from Fuzhou University, Fuzhou, China, in 1989, the M.Sc. degree in remote sensing of geology from China University of Geosciences, Wuhan, China, in 1992, and the Ph.D. degree in geology from the Institute of Geology, Chinese Academy of Sciences (CAS), Beijing, China, in 1998.

From 1992 to 2007, he was with the Information Processing Department, China Remote Sensing Satellite Ground Station (RSGS), CAS. In 2001, he became the Deputy Director of the Information Processing Department, RSGS, CAS. Since 2004, he has been a Professor and the Director of the Information Processing Department, RSGS, and also the head of the research group of Remote Sensing Information Mining and Intelligent Processing. From 2008 to 2012, he was a Professor and the Director of the Value-added Product Department and the Deputy Director of the Spatial Data Center, Center for Earth Observation and Digital Earth, CAS. Since 2013, he has been a Professor and the Director of the Satellite Data Based Value-added Product Department and the Deputy Director of RSGS, Institute of Remote Sensing and Digital Earth, CAS. A large part of his earlier research dealt with information processing and applications of satellite remote sensing data. His current research interests are focused on optical high-resolution remote sensing image understanding as well as using information retrieved from satellite remote sensing images in combination with other sources of data to support better understanding of the Earth.